Supplementary Information for

The Room-Temperature Ferromagnetism of 2H-SiC-α-Al_2O_3 Solid Solution Nanowires and the Physical Origin

Yong Sun, Cheng Lu, Hao Cui, Jing Wang, Yanming Ma, Chengxin Wang**

Dr.Y. Sun, Dr. H. Cui, Prof. J. Wang, Prof. C. X. Wang
State key laboratory of optoelectronic materials and technologies, School of Physics Science and Engineering, Sun Yat-sen (Zhongshan) University, Guangzhou 510275, People's Republic of China.E-mail: wchengx@mail.sysu.edu.cn
Dr. C. Lu, Prof. Y. M. Ma
State Key Lab of Superhard Materials, Jilin University, Changchun 130012, People's Republic of China.E-mail: mym@jlu.edu.cn (Y. M. M)

Supplementary Figure S1. TEM characterization of a SiC-Al_2O_3 nanowire after being immersed in 1M NaOH solution for 72 hours. (a) A TEM image with low-magnification. (b, c) the intermediate magnification images of the nanowire. (d) A single nanowire with thicker C layer. (e, f) EDS results corresponding to yellow and red areas.

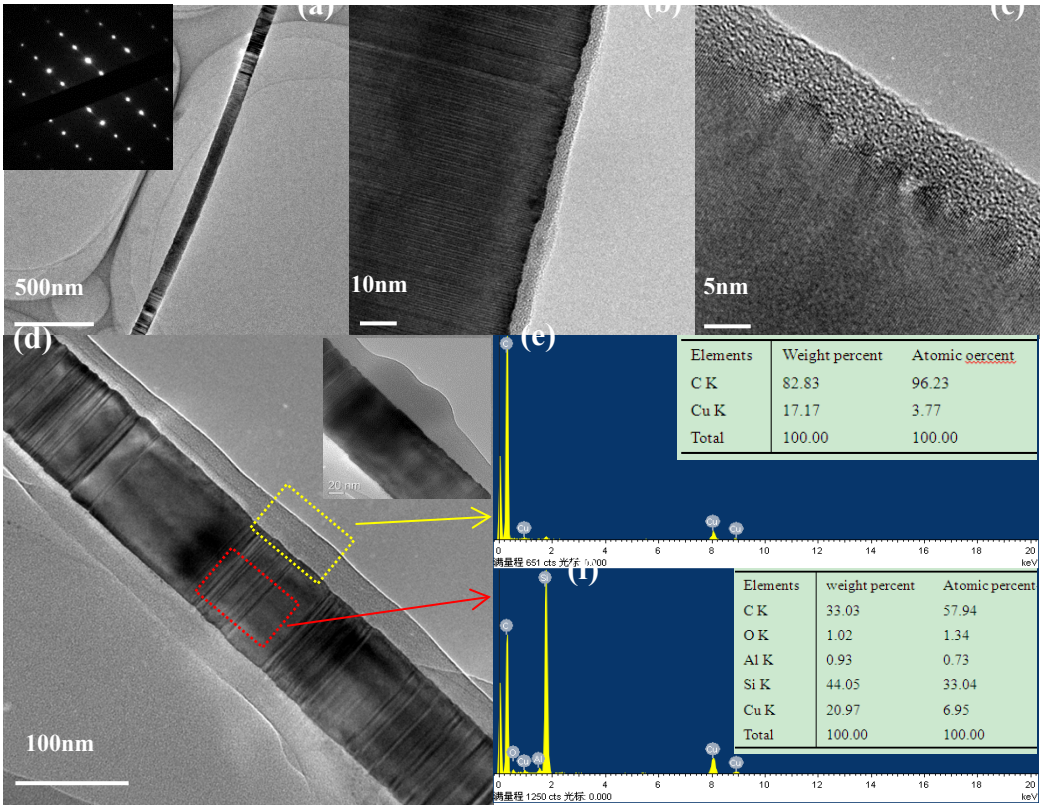

Supplementary Figure S2. (a1-a5) the XPS results collected from the pure SiC-Al_2O_3 solid solution nanowires paper after etching 2nm. (b1-b5) data collected after 20nm etching.

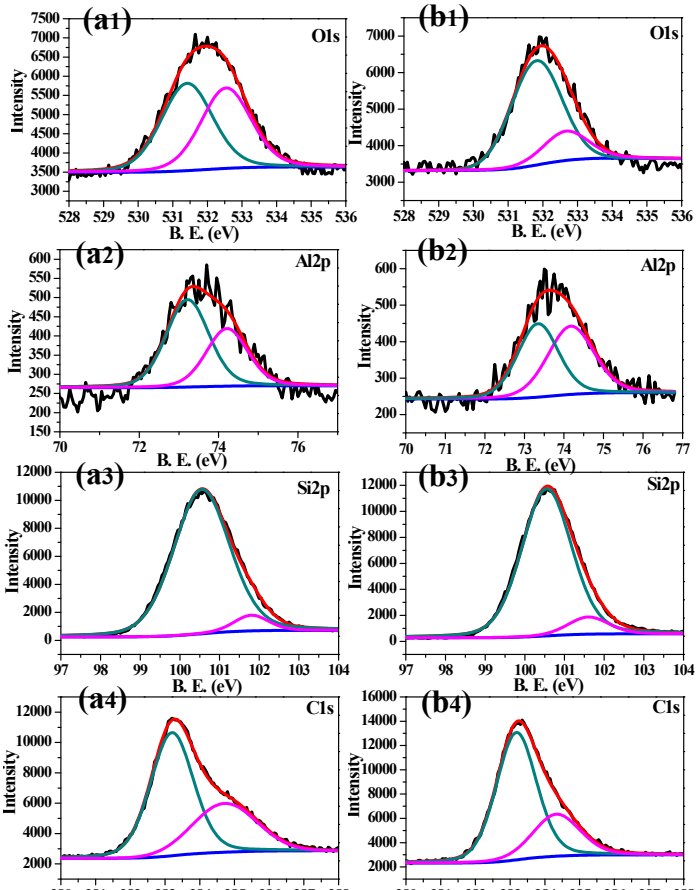

(a5)

Elements		At. %
C1s		51.78
O1s		8.36
Si2p		39.23
Al2p		0.63

(b5)

Elements		At. %
C1s		49.86
O1s		7.87
Si2p		40.19
Al2p		0.59
Ar		1.49

531.45eV and 532.55eV can be attributed to the binding energy of O1s in Al-O, C-O and Si-O bonds respectively. The binding energies of 73.24eV and 74.23eV correspond to Al2p orbit in Al-C and Al-O configurations. For Si2p, 100.55eV and 101.85eV were detected, indicating the presence of Si-C and Si-O bonds. In the C1s detection, C-Si (283.2eV) and C-C (284.75) signals is dominated; the latter one points to the residual amorphous carbon shell although mild etching process has been applied. Noticeably, most of the binding energy position is shifted comparing with completely pure phase, resulted from influence of other bonds. For example, Al-O bond in Al_2O_3 with binding energy of 74.7eV is located at 74.23eV alternatively as a result of the presence of Al-C band. Panel (b) is the XPS curves collected after etching 20nm, in which we can find the similar chemical states information. Moreover, the quantitive results from different depth levels shown in (b1) and (b2) further

confirm that Al and O elements are doped into SiC body with complex bonds forming.

Supplementary Figure S3. TEM characterization of a SiC-Al_2O_3 heterostructure. (a) Bright-field image at a relatively large magnification. (b) A nanowire with a broken Al_2O_3 side as a result of continuous electron-beam bombardment; the inset is the quantification of the EDS analysis collected from the region marked by the red circle. (c) An STEM image of a nanowire. (d) Elemental maps of Si, C, Al, and O.

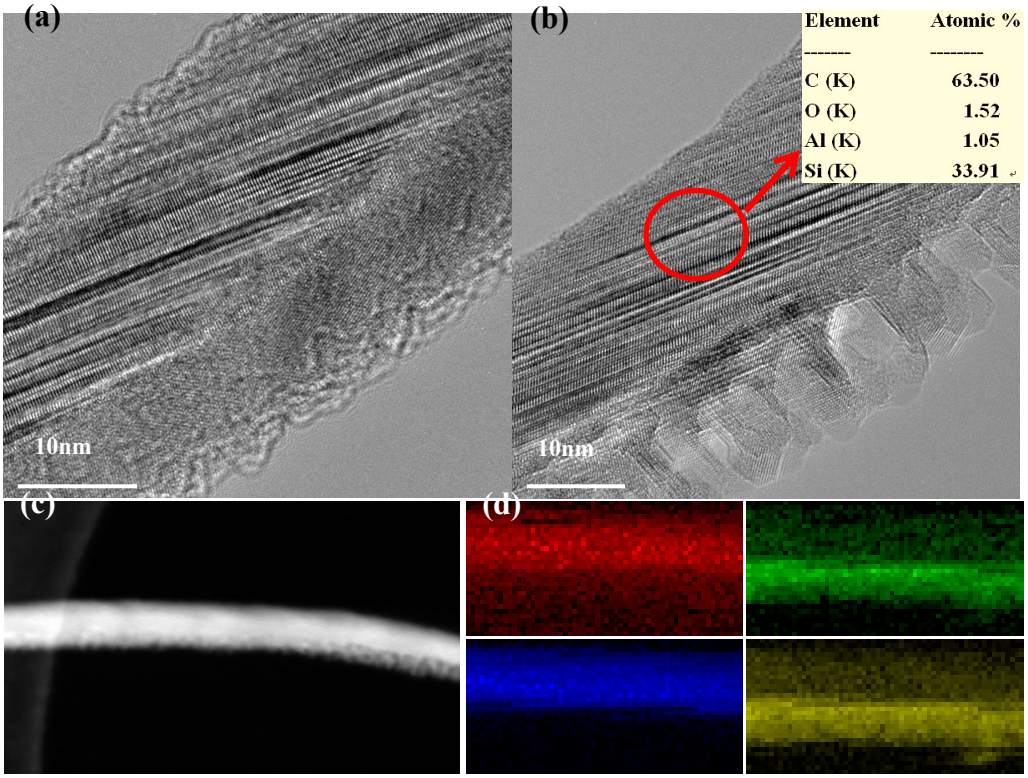

The nanowire presented is a longitudinal heterojunction between α-Al_2O_3 and 2H-SiC. EDS line scanning and SAED were used to expose the structural information and elemental distribution. The inset of **Supplementary Figure S2**(b) shows that ~1 mol% Al and ~1.5 mol% O were included in the SiC side, which approximately indicates the upper limit of Al_2O_3 present in the 2H-SiC-Al_2O_3 incomplete SS. Notably, **Supplementary Figure S2** (b) displays a broken Al_2O_3 side that was destroyed by the electron beam because of the weak crystallization of the precipitated Al_2O_3 crystal.

Supplementary Figure S4. TEM characterization of a type of SiC-Al_2O_3 heterostructural nanowire. (a) A TEM image with intermediate magnification. (b, c) SAED patterns corresponding to the area marked using the green and red circles. (d) The HRTEM image of one side of the nanowire; the red and yellow squares mark the SiC and Al_2O_3 lattices, respectively. (e,f) Fourier-transformation patterns corresponding to the lattice in (d).

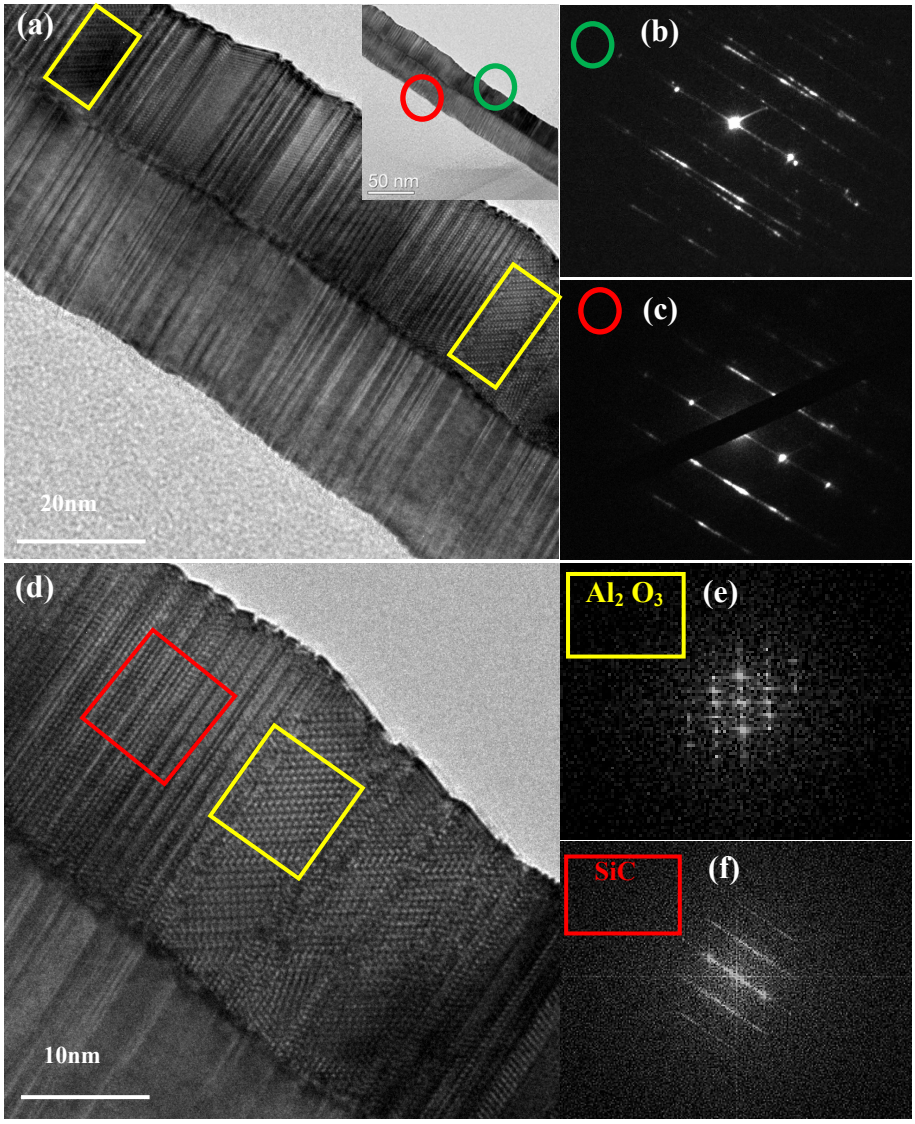

Another interesting configuration is shown here, where one side is 2H-SiC and the other side is an Al_2O_3-SiC superstructure. (b) and (c) show SAED patterns that correspond to the areas marked by red and green circles. Part (c) suggests that the red area is 2H-SiC, whereas the green part includes two types of patterns. HRTEM analysis revealed two different lattices. The Fourier-transform patterns corresponding to the two lattices are marked with red and yellow squares. On the basis of (e) and (f), we conclude that the red square represents 2H-SiC and that the yellow area represents α-Al_2O_3.

Supplementary Figure S5. (a1-a3) the FC-ZFC curves of samples with different Al_2O_3 content in the solid solution phase. (b1-b3) corresponding SEM images of the three samples.

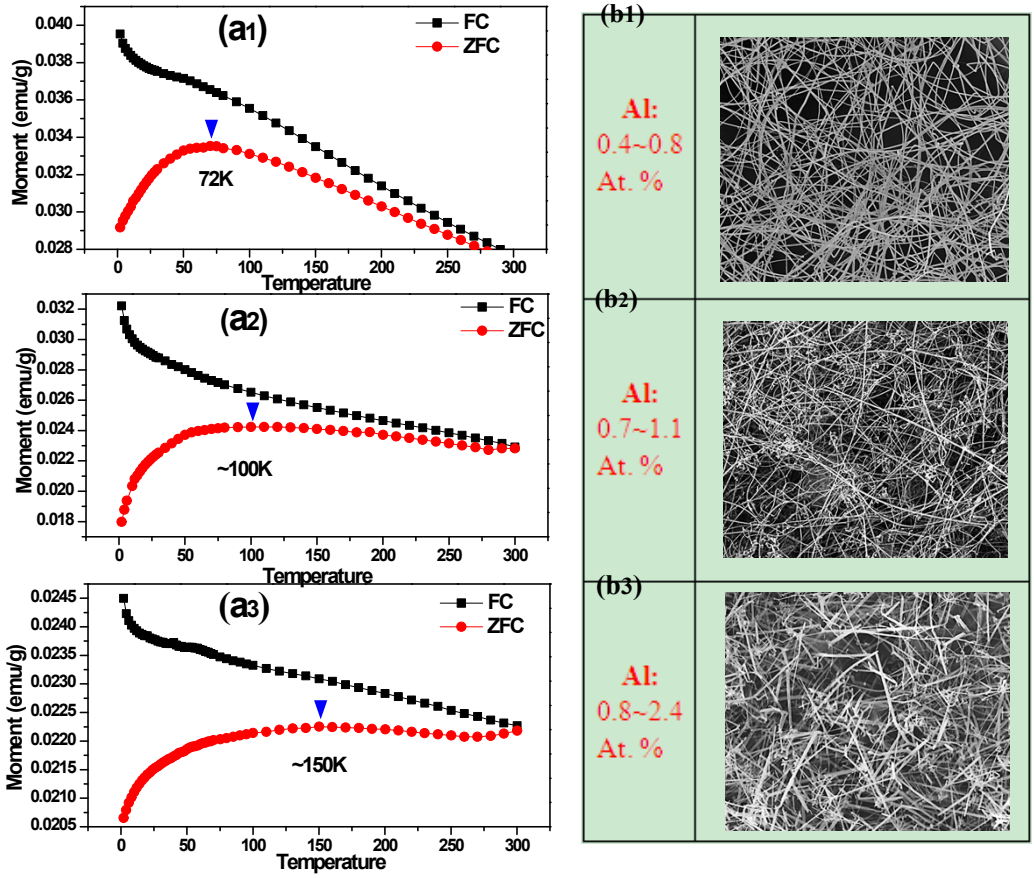

In order to supply a clear image between the magnetism and Al_2O_3 component, we managed to realize different doping concentration on several levels and investigated their magnetic behavior. Noticeably, high Al concentration would result in impurities like Al_2O_3 and Al_4C_3 as a result of excessive Al supplement. In this case, it is not competent for XPS method to be used to analyze the Al content. Herein, tens of single nanowires were picked and investigated under TEM. We provide a statistical Al concentration range as shown in **Supplementary Figure S5** (b1-b3). It seems that the results of the Al contents acquired using XPS and EDS methods agree well by comparing the data from pure 2H-SiC-Al_2O_3 solid solution nanowires paper. It is worthy to be mentioned that more Al_2O_3 component in solid solution nanowires may not result in higher magnetization intensity by comparing the three cases, which originate from the impurities that is non-magnetic or diamagnetic.

Supplementary Table S1. The calculated relative energies ΔE, energy differences, ΔE_m between AFM and FM, and the magnetic moment μ for each configuration of the 2H-SiC-Al_2O_3 SS (model 3 in **Figure** 5(a)). For each structure, the energy of the lower-energy state (either FM or AFM) of the optimized model is given with respect to the lowest optimized energy structure with the same elements, i.e., $\Delta E_7 = E$ (vacancy 7) - E (vacancy 2)。 Vacancy 2 is the lowest optimized energy structure.

Si vacancy	μ (μ_B)	ΔE_m (meV)	ΔE (eV)
1	2.008	-0.0008	2.0683
2	2.038	128.1817	0
3	1.986	-0.0044	0.3617
4	2.012	195.6764	0.7642
5	0	0.0010	0.1786
6	0	0.0011	0.2813
7	0.001	-0.0010	0.2492

Theoretical calculations. The present calculations were performed using the Perdew-Burke-Ernzerhof (PBE) parameterization of the general gradient approximation (GGA),[1] as implemented in the Vienna Ab Initio Simulation Package (VASP).[2] The electron and core interactions were included using the frozen-core all-electron projector-augmented wave (PAW) method,[3] with C $2s^2 2p^2$ (cutoff radius 1.50 *a.u.*), O $2s^2 2p^4$ (cutoff radius 1.52 *a.u.*), Al $3s^2 3p^1$ (cutoff radius 1.90 *a.u.*), and Si $3s^2 3p^2$ (cutoff radius 1.90 *a.u.*) treated as valence electrons. A cutoff energy of 500 eV was used for the expansion of the electronic wave function into plane waves. Special k points were generated with a 4 × 4 × 4 grid on the basis of the Monkhorst-Pack scheme.[4] Good convergence was obtained with these parameters; the total energy converged to better than 1 meV/atom. The symmetry-unrestricted optimizations for geometry were performed using the conjugate gradient scheme until the maximum force allowed on each atom was less than 0.001 eV/Å.

We performed the calculations by considering three models of a 72-atom 3 × 3 × 2 2H-SiC super cell, as shown in **Figure 5**(a). The three models of the 2H-SiC-Al_2O_3 SS super cell were based on the following conditions: In the replaced model (1), two Si atoms were randomly replaced with two Al atoms and three C atoms were replaced by three O atoms ($2Al_{Si} + 3O_C$). In the C vacancy defect model (2), two Si atoms were randomly substituted with two Al atoms and three C atoms were substituted with three O atoms; in addition, one C atom was removed ($2Al_{Si} + 3O_C + V_C$). In the Si vacancy defect model (3), two Si atoms were randomly substituted with two Al atoms and three C atoms were substituted with three O atoms; in addition, one Si atom was removed ($2Al_{Si} + 3O_C + V_{Si}$), which is identical to the previously described configuration of the SS.

References

[1]Perdew, J. P.; Burke, K.; Ernzerhof, M. Generalized Gradient Approximation Made Simple. *Phys. Rev. Lett.* **1996**, *77*, 3865-3868.

[2]Kresse, G.; Furthmüller, J. Efficient iterative schemes for ab initio total-energy calculations using a plane-wave basis set. *Phys. Rev. B,* **1996**, *54*, 11169-11186.

[3]Blöchl, P. E. Projector augmented-wave method. *Phys. Rev. B*, **1994**, *50*, 17953-17979.

[4]Monkhorst, H. J.; J. D. Pack, Special points for Brillouin-zone integrations. *Phys. Rev. B*, **1976**, *13*, 5188-5192.